Dual-Function Nanofilm Coatings with Diffusion Control and Protein Resistance

Jaebum Park[†] and Michael J. McShane[*,†,‡]

Materials Science and Engineering Program and Department of Biomedical Engineering, Texas A&M University, College Station, Texas 77843

ABSTRACT To date, limited examples of polyelectrolyte multilayers (PEMs) can be found that truly exploit the power of layer-by-layer nanoassembly to combine multiple functions into a complex multilayer. We demonstrate that PEMs can be designed as optimized coatings for implantable biosensors, exhibiting both diffusion control and protein resistance. PEM coatings comprising strong−weak and weak−weak pairs were evaluated, resulting in decreases in glucose diffusivity up to 5 orders of magnitude compared to water. Addition of poly(ethylene glycol) (PEG)-grafted terminal layers on the base diffusion-controlling multilayers substantially improved resistance to albumin adsorption relative to unmodified PEMs. For transport-controlling films comprising strong−weak polyelectrolyte pairs, the consistent diffusivity was observed even after exposure to protein-containing solutions, indicating minimal effects of biofouling. In contrast, the transport behavior of weak−weak polyelectrolyte pairs was susceptible to alteration by protein exposure, resulting in large variation in diffusivity, even when protein-resistant outer layers were employed.

KEYWORDS: nanofilms • polyelectrolyte multilayers • layer-by-layer self-assembly • biosensors • biocompatibility

INTRODUCTION

Implanted medical devices, especially biosensors, require proper biointerfaces that prevent surface fouling and host response initiation while maintaining control over the transport of molecules into the implant. In enzymatic biosensors that operate on the basis of substrate flux, a transport-limiting membrane is typically employed, often in the form of a coating applied to the reactive enzyme phase. Such enzymatic biosensors require incorporation of a diffusion-limiting coating to balance the flux of incoming substrates with reaction kinetics to obtain a measurable signal over the desired response range (1). The transport-limiting coating may also reduce the rate of substrate consumption, which can be important for biological or biomedical applications where perturbation of the sensor surrounding needs to be minimized to avoid nutrient deprivation of cells. Demonstration of self-assembled multilayer films that meet this dual requirement is the focus of this report, where diffusion-controlling materials are combined with a biofouling-resistant (protein adsorption-resistant) outer layer.

Glucose sensors have emerged as prime examples of this technology, where typical devices operate based on the oxidation of glucose driven by glucose oxidase (GOx) (2). However, physiological glucose levels are 2.3−23 mM (supplied via diffusion from capillaries) while oxygen levels range from 0−277 μM (supplied via diffusion from the atmosphere and diffusion from capillaries) (3−5); under these conditions, membranes of low relative glucose diffusivity are required to balance oxygen and glucose transport to obtain a glucose-limited response. A wide variety of materials have been proposed to provide this control, including poly(dimethylsiloxane) (PDMS) (6, 7), Nafion (8−11), nanoporous silicon membranes (12), and polyethylene-*block*-polystyrene (13).

Although these materials have performed well in macroscale sensors, the options for transport-controlling coatings become very limited when materials amenable to self-assembly are required, such as for devices with all dimensions at a scale where individual manipulation is impractical (e.g., microspheres, nanoparticles). When attempting to shrink the size of biosensors to the level that self-assembly is used to fabricate the devices, two major difficulties arise for the choice of materials. First, achieving the necessary balance of diffusion and reaction becomes increasingly difficult because the overall diffusion lengths are extraordinarily small; thus, membranes that provide even lower diffusivity are required. Second, the selection of materials depends on the methods used for fabrication, and this immediately rules out certain classes of materials, because there are no suitable approaches to deposit these materials with micro/nanoscale precision on the enzyme included matrices. There is an optimal range of transport barrier, a combination of thickness and diffusion coefficient, for a given sensor interior matrix, size, enzyme concentration, reaction scheme, and analyte concentration that maximizes sensitivity while ensuring diffusion-limited behavior over the range of interest.

An attractive possibility to construct such transport-limiting coatings is the layer-by-layer (LbL) self-assembly technique because of the flexibility of the approach to create composite films with nanometer resolutionof thickness (14, 15). Bruening et al. published a series of reports describing the transport of various molecular species through polyelectrolyte multilayers (PEMs) (16−18). In one report,

* Corresponding author. E-mail: mcshane@tamu.edu.
Received for review October 6, 2009 and accepted March 11, 2010
† Materials Science and Engineering Program, Texas A&M University.
‡ Department of Biomedical Engineering, Texas A&M University.
DOI: 10.1021/am900673r

Scheme 1. Schematic Diagram of Dual-Functional Nanofilms Comprising PEMs and PEG-Terminated PEMs, Exhibiting Both Diffusion Control and Resistance to Protein Adsorption

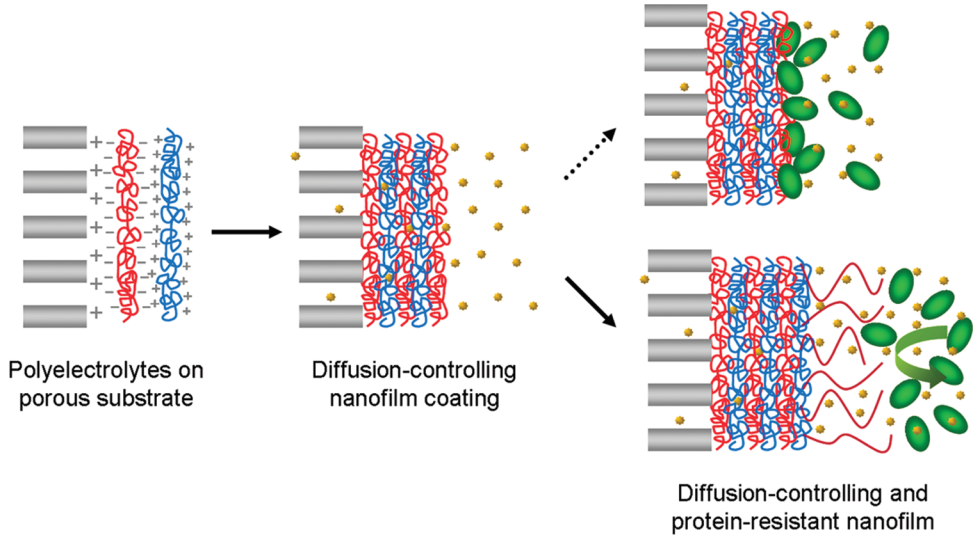

the transport of uncharged solutes such as glucose, glycerol, and sucrose through polyelectrolyte multilayers with various film architectures was explored, and results demonstrated that the glucose diffusivity through "model" PEMs (9.87×10^{-10} cm^2/s) was 4 orders of magnitude smaller than glucose diffusivity in water (6.9×10^{-6} cm^2/s) (16). Exploiting this extraordinarily low glucose diffusivity and precision for assembly, we have successfully applied LbL films as tunable diffusion-limiting coatings for optical biosensors (19, 20).

PEMs possess inherent nanocomposite structure, which provides for the interesting possibility of designing PEMs with more than one function (21). PEMs constructed by LbL self-assembly are also extensively used in various biomedical applications such as drug delivery systems (22−24), and cell engineering (25−27). However, proteins strongly interact with the polyelectrolyte film regardless of sign of the charges of both the multilayer and the protein (28), and protein adsorption is the initial event that mediates host response to foreign materials (29). To further make systems appropriate for in vivo deployment, it is essential to create an interface with the biological system that minimizes the response to the foreign material, such as inflammation and immune system attack. Masking implants to avoid protein adsorption enhances biocompatibility and minimizes fouling of surfaces which may alter substrate flux, shifting sensor response profiles. Poly(ethylene glycol) (PEG) is well-known to resist protein adsorption (30), and can be immobilized on surfaces via hydrogen bonding (31), covalently attachment (32), or ionic interaction (33). In this work, poly(L-lysine)-*graft*-PEG (PLL-*g*-PEG) was chosen for surface modification, as a surface "comb" of PEG has been thoroughly evaluated for toxicity, immunogenicity, pyrogenicity, and biodegradation (34, 35). This copolymer electrostatically adsorbs to the anionic surface of poly(styrene sulfonate) (PSS) or poly(acrylic acid) (PAA)-terminated PEMs that is compatible with the LbL process without using chemical cross-linking reagents (which is preferred when treating particles with biological activity that must be preserved), and be more stable at a broad range of pH than H-bonded films.

Determining the transport property of nanofilms with different compositions of materials is critical for in vivo applications of biomedical devices. We hypothesized that an outer layer of protein-resistant material could be applied to an inner layer of glucose transport-limiting material to achieve this dual functionality. To test this hypothesis, we compared different nanofilms deposited on porous substrates. We applied PEG-modified polyelectrolyte coatings to nanofilms designed for transport control (Scheme 1), and the diffusion and protein adsorption of the native transport-control films were compared with the PEG-modified versions before and after exposure to albumin solutions and serum.

MATERIALS AND METHODS

Materials. PSS ($M_w = 70\,000$), poly(allylamine hydrochloride) (PAH, $M_w = 70\,000$), PAA ($M_w = 100\,000$, 35 wt % in water) and poly(ethyleneimine) (PEI, $M_n \approx 60\,000$, 50 wt % in water) were purchased from Aldrich. Glucose, GOx, peroxidase, o-dianisidine, NaCl, NaOH, HCl, poly(L-lysine) (PLL, $M_w = 12\,000$−$24\,000$), and bovine serum albumin (BSA) were purchased from Sigma. PLL-*g*[4.5]-PEG (PLL = 20 kDa; PEG = 5 kDa; Lys/PEG graft ratio = 4.5) was purchased from Alamanda Polymers, Inc. Fetal bovine serum (FBS) was purchased from Cascade Biologics. The porous alumina supports (Anodisc 25, 60 μm thick, 0.02 μm pore diameter) were purchased from Whatman Ltd. Deionized water (>18.2 MΩ cm) was always used for preparation of polyelectrolyte solutions and rinsing. The pH of the polyelectrolyte solutions was adjusted with either HCl or NaOH.

Layer-by-Layer (LbL) Self-Assembly of Nanofilms. PSS/PAH deposition started with exposure of one side of the alumina support using open-face filter holder (Pall Co.) in 0.02 M PSS (molarities of polyelectrolytes are given with respect to the repeating unit) in 0.5 M NaCl solution adjusted to pH 2.1 for 5 min. The alumina support was rinsed with deionized water for 1 min before exposure to 0.02 M PSS in 0.5 M NaCl adjusted to pH 2.3 for 5 min, followed by another water rinse for 1 min. PAA/PAH alternative adsorptions involved same deposition and rinse time with 0.02 M PAA (pH 5.5, 0.5 M NaCl) and 0.02 M PAH (pH 5.5, 0.5 M NaCl). We repeated this process until the target number of layers was achieved (more than 5 bilayers are

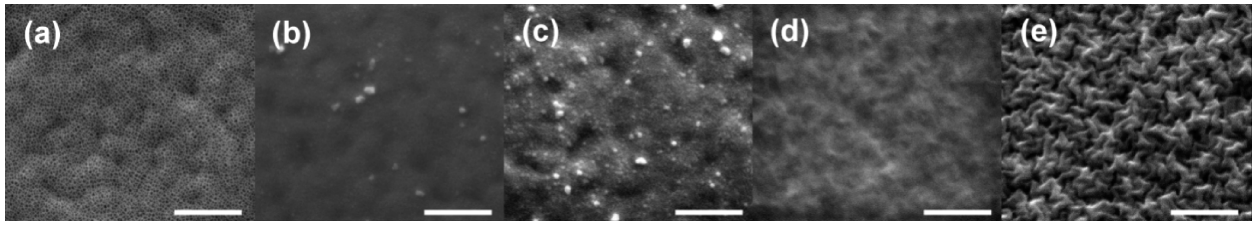

FIGURE 1. Scanning electron microscope images of nanofilms: (a) bare alumina substrate; (b) [PSS/PAH]$_6$PSS; (c) [PSS/PAH]$_6$PSS/PLL-*g*-PEG; (d) [PAA/PAH]$_6$PAA; and (e) [PAA/PAH]$_6$PAA/PLL-*g*-PEG. Samples were coated with 5 nm of platinum prior to imaging. All scale bars are 1 μm.

required because of the sufficient surface coverage of PEM) (36). Deposition pH of PAA/PAH followed previous reports, which required conditions of pH higher than 5.0 for PAA adsorption solution, and pH lower than 7.5 for PAH solution (37−39). These conditions optimize the polyelectrolyte deposited in a highly charged state and colloidal stability, when applied to particle-base biochemical sensor coatings. The PLL and PLL-*g*[4.5]-PEG depositions involved a 5 min exposure in PLL (1 mg/mL in phosphate buffered saline (PBS)) and PLL-*g*[4.5]-PEG (1 mg/mL in PBS) solutions on top of either PSS or PAH terminal layer. Films were dried with N_2 only after deposition of all layers.

Different combinations of nanofilm assemblies were characterized by scanning electron microscope (SEM, Quanta 600 FE-SEM, FEI Company) and quartz crystal microbalance (QCM, QCM200, Stanford Research Systems, Inc.). Static (θ_{static}) contact angle (CA) measurements of deionized water droplets at the nanofilm−air interface were measured at room temperature using goniometer (CAM200, KSV Instruments, Ltd.) with measuring a 3 μL sessile drop of water at 30 s after deposition onto the nanofilm surfaces. Thickness and refractive index was measured by ellipsometry (EP3-SE, Nanofilm, Inc.) with an incident angle of 54° and a wavelength of 532 nm in a four-zone compensator mode to minimize errors in surface homogeneity.

Measurements of Protein Adsorption. AT-cut quartz crystals with a fundamental resonance frequency of 5 MHz were cleaned by immersion into a 1:1:5 solution of H_2O_2 (30% w/w), NH_4OH (25% w/w), and deionized water heated to a temperature of about 75 °C for 5 min followed by immediately rinse with deionized water and drying with N_2. The gold surface of the quartz crystal was immersed for 10 min in 0.02 M PEI solution containing 0.5 M NaCl to create a positively charged substrate surface. Then LbL deposition of nanofilms was conducted following the same procedure as above. The quartz crystal was rinsed by deionized water for 1 min before loading to the QCM liquid flow cell. Flow through the QCM cell coated with nanofilm was present during the all frequency measurements including stabilization, protein adsorption, and rinsing steps. Either BSA (1 mg/mL in PBS) or FBS (used as purchased) solution was introduced into the flow system for 1 hour after rinsing and stabilizing the QCM frequency, and frequency shifts were continuously monitored after rinsing with PBS. The mass was determined from the measured frequency using Sauerbrey's equation (40).

Diffusion Measurements. Three parallel horizontal diffusion cells (Permegear, Inc.) were used to study the transport of glucose molecules through the polyelectrolyte nanofilms. Each cell consists of two parts, feed and permeate chambers. The alumina support, coated with the film of interest, was placed in between the chambers. The nanofilms were presoaked into 0.4 mM glucose in PBS solution (same solution as feed side when diffusion experiment is conducted) for 12 h to equilibrate glucose concentration between film and solution phases. The permeate chamber was replaced with PBS, and the feed chamber contained 0.4 mM glucose in PBS. At this time, a drive with a high-precision multichannel pump (IPC-N, Ismatec) withdrew liquid synchronously from both feed and permeate chambers to maintain constant volume, and temperature of the diffusion cells were maintained by water circulator at 27 °C. The sampled permeate solution transferred to a 96-well plate through the fraction collector (FC 203B, Gilson, Inc.). All operations were performed with control provided by a computer running custom LabVIEW virtual instrumentation. Glucose concentration was measured after 30 min incubation at 37 °C by plate reader (Infinite F200, Tecan, Ltd.) with adding reaction mixture of glucose oxidase, peroxidase, and *o*-dianisidine (41).

RESULTS AND DISCUSSION

Many biosensors require control over both analyte permeability and interaction with the biological environment, such as soluble proteins. Adsorption of proteins on biomaterial surfaces is called fouling, a process that results in "clogging" of pores and, consequently, reduced transport into the material. This is a severe problem for biosensors that rely on analyte flux, because changing permeability will result in altered sensitivity and dynamic range for the sensor response. Therefore, we explored the possibility of combining PEMs with known low glucose permeability with additional outer layers to enhance their resistance to protein adsorption.

Previous work demonstrated PEG-grafted polyelectrolytes with appropriate grafting ratio and length of PEG had strong resistance to nonspecific protein adsorption (33−35, 42, 43). We used PLL-*g*-PEG to modify the surface of [PSS/PAH]$_6$PSS, and [PAA/PAH]$_6$PAA nanofilms, and compared their protein resistance in the presence of BSA. Using glucose as a model analyte, we then determined diffusion coefficients (*D*) through various nanofilms using an automated testing apparatus, which permeated sample passing through the nanofilms immobilized on porous substrate. *D* values were extracted by regression of flux and concentration gradient data using Fick's first law.

Nanofilms were assembled on bare alumina substrates. PSS (strong polyanion), PAA (weak polyanion), PAH (weak polycation), PLL (weak polycation), and PLL-*g*-PEG were used as film components. The assemblies were characterized by SEM (Figure 1 and the Supporting Information), ellipsometry (Figure 3, Table 2), contact angle measurements (Table 1), and QCM (see the Supporting Information). As observed via SEM, all pores were covered by PEMs after LbL self-assembly, and the different nanofilms possess very different morphology contributed by the different interactions between weak-strong and weak−weak polyelectrolyte pairs as well as the grafted PEG side chains (Figure 1b−e and the Supporting Information).

We directly determined protein uptake on the different films ([PSS/PAH]$_6$PSS, [PSS/PAH]$_6$PSS/PAH, [PSS/PAH]$_6$PSS/

Table 1. Static (θ_{static}) Contact Angle (CA) Measurements of Deionized Water Droplets at the Nanofilm–Air Interface

Film Composition	*CA* (°C)
$[PSS/PAH]_6PSS$	49 ± 1
$[PSS/PAH]_6PSS/PAH$	58 ± 1
$[PSS/PAH]_6PSS/PLL$	42 ± 1
$[PSS/PAH]_6PSS/PLL$-*g*-PEG	28 ± 1
$[PAA/PAH]_6PAA$	58 ± 1
$[PAA/PAH]_6PAA/PAH$	62 ± 1
$[PAA/PAH]_6PAA/PLL$	63 ± 1
$[PAA/PAH]_6PAA/PLL$-g-PEG	39 ± 3

PLL, and $[PSS/PAH]_6PSS/PLL$-*g*-PEG) via QCM (Figure 2a). Real-time protein adsorption after BSA introduction on the different nanofilms indicated that almost 90% of adsorption takes place within 5 min. QCM measurements of mass changes indicated a substantial improvement in adsorption resistance with the addition of the final PLL-*g*-PEG layer. PLL-*g*-PEG coatings were the most resistant to albumin adsorption of the films considered, and PEG decreases the albumin mass to below the detection limit of the technique (<45 ng/cm^2) compared to unmodified PSS (736 ± 52 ng/cm^2), PAH (567 ± 18 ng/cm^2), and PLL (658 ± 39 ng/cm^2) (Figure 2b).

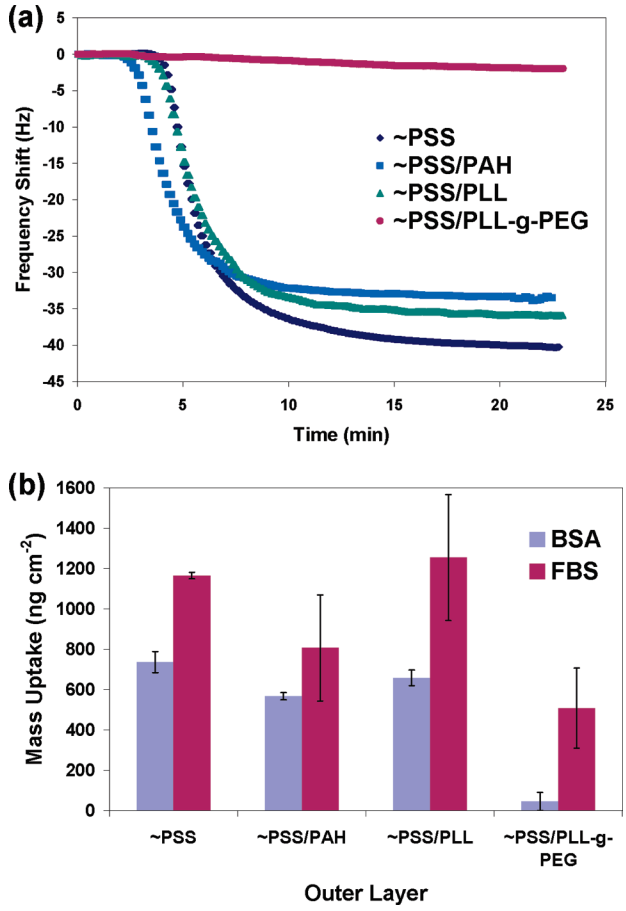

FIGURE 2. (a) Real-time QCM frequency shifts after BSA introduction on the different nanofilms; (b) mass uptake to nanofilms with different outermost layers on top of the base-$[PSS/PAH]_6$ multilayer, measured by QCM after exposure of BSA and FBS. PLL-*g*-PEG outer layer improved resistance to BSA ($p < 0.005$), but less dramatic improvement in serum ($p < 0.1$).

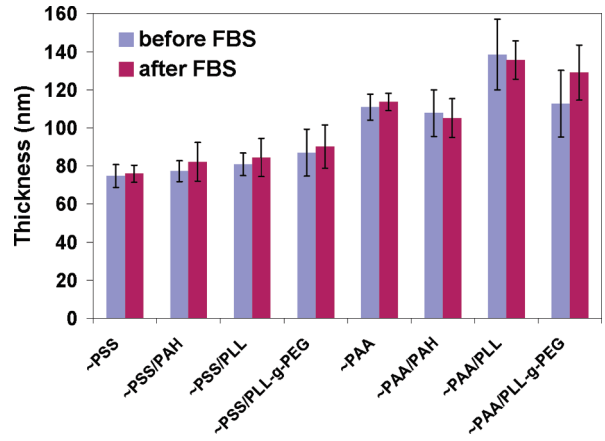

FIGURE 3. Nanofilm thickness with different outermost layers before and after immersing in FBS, as measured by ellipsometry. All films were measured in dry state. The first half of the *x*-axis indicates final layer set on top of $[PSS/PAH]_6$, and the second half indicates final layer set on top of $[PAA/PAH]_6$ on the alumina substrate. Error bars indicate one standard deviation from five measurements.

This is consistent with previous reports on PEGylation for similar materials (33, 35, 44). Interestingly, the quantity of protein adsorption on the unmodified films was not directly related with charge of the surface layer and only weakly correlated with the contact angle of the films (correlation coefficient, ρ(CA, mass uptake) = 0.77). In all nanofilms, the adsorbed mass increases after FBS exposure were higher than those due to BSA, indicating serum proteins and potentially other molecules in the serum attach to or penetrate into nanofilms (45, 46), and may also change the environment (e.g., viscosity, charge density) around PEMs on the quartz crystal electrode. Surprisingly, investigations of protein adsorptions on [PAA/PAH]-base films with different final layers revealed unstable signals from QCM after protein solution was introduced even for PEG-terminated films, indicating the susceptible nature of the underlying PEMs. It is noteworthy that the sensitivity of weak–weak polyelectrolyte pairs to environmental changes has been previously observed to depend on assembly pH as well as humidity (47–49).

The thickness of different multilayers on the porous alumina substrate was measured by ellipsometry (Figure 3). It was observed that the thickness before and after serum exposure was not statistically different in any films, despite the apparently large changes observed via QCM; this was expected, since the native nanofilms were ~100 nm, and an added layer of proteins adsorbed onto the nanofilm surface would add only 5–10 nm. However, the thickness of [PSS/PAH]-base films (strong-weak PE interaction) and [PAA/PAH]-base films (weak–weak PE interaction) were different ($p < 0.01$) regardless of serum adsorption. These ellipsometry results provide evidence that weak–weak PEMs are thicker and highly interpenetrated structure than strong-weak PEMs, and this is compatible with previous reports (47, 48). It is also noteworthy that none of the coatings exhibited a decrease in thickness because of protein exposure, suggesting that the environment of the protein-containing solutions does not result in disintegration of the nanofilms.

Table 2. Thickness (d), Refractive Index (n) of Nanofilms, and Diffusion Coefficients (D) of Glucose through Nanofilms

nanofilm composition	d (nm)[a]	n[b]	$D_{glucose}$ ($\times 10^{-10}$ cm^2/s)[c]
$[PSS/PAH]_6PSS$	74.7 ± 6.0	1.52 ± 0.004	4.61 ± 0.37
$[PSS/PAH]_6PSS/PAH$	77.2 ± 5.5	1.51 ± 0.008	3.93 ± 0.28
$[PSS/PAH]_6PSS/PLL$	80.8 ± 5.9	1.51 ± 0.005	4.03 ± 0.22
$[PSS/PAH]_6PSS/$ PLL-g-PEG	87.0 ± 12.3	1.51 ± 0.007	2.54 ± 0.22
$[PAA/PAH]_6PAA$	110.8 ± 6.8	1.44 ± 0.006	0.99 ± 0.07
$[PAA/PAH]_6PAA/PAH$	107.7 ± 12.2	1.46 ± 0.007	0.26 ± 0.06
$[PAA/PAH]_6PAA/PLL$	138.5 ± 18.5	1.47 ± 0.019	1.01 ± 0.06
$[PAA/PAH]_6PAA/$ PLL-g-PEG	112.7 ± 17.5	1.45 ± 0.008	0.22 ± 0.02

[a] Average thickness (d) values measured by ellipsometry were used as dx in D calculations, and feed gradient dC/dx assumed constant for linear permeate concentration increase. [b] Refractive index of the bare alumina substrate was 1.35. [c] The value of glucose through bare alumina substrate was 1.15×10^{-6} cm^2/s.

Nanofilm coatings decreased D of glucose up to 5 orders of magnitude, and [PAA/PAH]-base films generally decreased D values of glucose more than [PSS/PAH]-base films did. Previous reports have shown that additional one PAH terminal layer ($[PSS/PAH]_7$) relative to PSS-terminated film ($[PSS/PAH]_6PSS$) slightly decreased flux of glucose due to the tighter surface packing of PAH, and the flux of glucose through 5 bilayers of PSS/PAH capped with 1.5 bilayers of PAA/PAH/PAA ($[PSS/PAH]_5[PAA/PAH]PAA$) was 30-fold lower than for $[PSS/PAH]_6PSS$ film (16, 20). Our D values for $[PSS/PAH]_6PSS$ and $[PSS/PAH]_6PSS/PAH$ corresponded with those observations, and D values of [PAA/PAH]-base films were significantly smaller than that of [PSS/PAH]-base films in general (Table 2). We also found that PEGylated surfaces maintained their diffusion property in the same order of magnitude as nanofilms with the same underlying composition.

Interestingly, all [PAA/PAH]-base films exhibited a different pattern of transport behavior due to the different surface packing of film and hydrophilicity of material. Unlike [PAA/PAH] capped [PSS/PAH] films in the previous work (16), the D value of PAA-terminated nanofilms ($[PAA/PAH]_6PAA$) was found to be higher than that of PAH-terminated nanofilm ($[PAA/PAH]_7$). We considered whether D values were correlated with contact angle, but found that diffusivity in [PAA/PAH]-base films was independent of contact angle ($\rho(D, CA) = -0.26$). On the basis of previous work, PAA/PAH PEMs formed under certain pH and ionic strength conditions can undergo morphological transformation to form micro/nanoporous films, by their post-treatment immersing into acidic solution (pH ~2.4) (50), and washing with salt solutions compared to pure water (51).

It has also been revealed that a pH-induced swelling transition from dense film to nanoporous films results in lower refractive indices in PAA/PAH films following acid treatment (52, 53), typically changing refractive index (RI) by 0.1−0.2 units. We measured refractive indices of all nanofilms on the alumina substrates to determine whether the [PAA/PAH]-based films exhibited changes in refractive

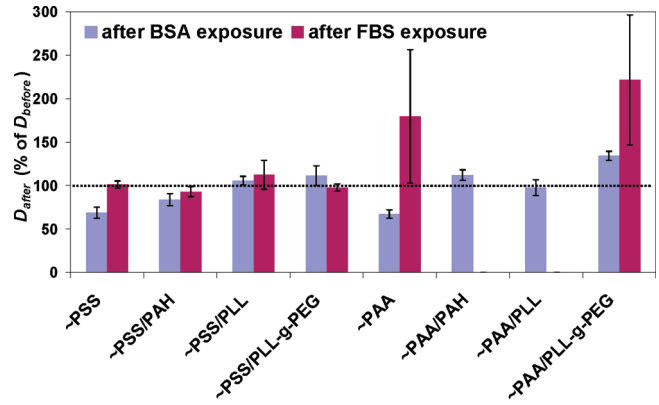

FIGURE 4. Change in glucose diffusivity in nanofilms after BSA and FBS exposure. The first half of the x-axis indicates final layer set on top of $[PSS/PAH]_6$, and the second half indicates final layer set on top of $[PAA/PAH]_6$. Each bar indicates relative % of mean D value after BSA and FBS exposures from D values of native nanofilm (100%, dashed line) before protein and serum exposures. Error bars represent the 95% confidence interval.

index that would suggest a transition to a nanoporous state (Table 2). We found that all of the [PSS/PAH]-based films had an average refractive index of 1.51, whereas refractive indices of [PAA/PAH]-base films had average values of 1.45. Both of these were found to be significantly different from the refractive index of the bare alumina substrate (1.35). However, the refractive indices of $[PAA/PAH]_6PAA$ films did not exhibit any significant change upon addition of capping layers of PLL or PLL-g-PEG. These observations indicate that surface modification with different polyelectrolytes does not induce a transition to a nanoporous state. This agrees with expectations, as the pH of the PLL and PLL-g-PEG solution used for adsorption was neutral.

On the basis of previous work and above results, we appreciate the fact that the structure of PAA/PAH multilayers can be affected by small change of environment. Our main concern is the susceptibility to changes in physiological conditions for in vivo applications, and particularly whether this susceptibility is altered by the presence of a "capping" layer of PLL-g-PEG, which theoretically would protect the underlying layers from interactions with large proteins. Our primary focus is on how the diffusivity of these weak−weak polyelectrolyte pairs can be affected before and after protein and serum exposure relative to strong-weak pairs. We observed that the underlying films played a more important role in the response to proteins, whether it was modified with protein-resistance surface or not.

After determining D values of glucose through various nanofilms, we investigated how transport properties of nanofilms are affected by protein adsorption on the films as might be experienced by implanted devices (Figure 4). Overall, D values of [PSS/PAH]-base films after protein and serum exposure had excellent correspondence with original D values of native films, particularly for PLL-terminated and PLL-g-PEG-terminated nanofilms. No statistical difference of D values was observed in between after protein exposure and serum exposure in the same composition of the films, except $[PAA/PAH]_6PAA/PAH$ and $[PAA/PAH]_6PAA/PLL$ films; these materials did not permeate glucose after serum expo-

sure (glucose concentration below the detection limit of colorimetric assay via plate reader). Glucose diffusivity in $[PSS/PAH]_6PSS/PLL$ and $[PSS/PAH]_6PSS/PLL$-*g*-PEG films was minimally affected after protein adsorption (+5.7%, +11.3% respectively) and serum exposure (+12.2%, −2.2%, respectively). Even though the diffusivity of $[PSS/PAH]_6PSS/PLL$ was not strongly influenced by protein exposure, it still has protein adsorption (Figure 2), which might mediate host responses in vivo applications. However, strong interactions with protein solutions were observed in all [PAA/PAH]-base films, with more dramatic changes after serum exposure. We also measured glucose diffusivity with $[PSS/PAH]_6PSS/PLL$-g-PEG, $[PAA/PAH]_6PAA$, and $[PAA/PAH]_6PAA/PLL$-g-PEG after exposure to serum for 24 h (see the Supporting Information). $[PSS/PAH]_6PSS/PLL$-g-PEG still maintains glucose diffusivity as we expected, whereas weak−weak PEMs are not stable.

On the basis of the protein adsorption experiment, we conclude [PAA/PAH]-base films were strongly affected by both protein and serum exposure even in the PLL-*g*-PEG finalized film, and the susceptible nature of these weak−weak PEMs caused large variation in *D* values of glucose. We also note that chemical cross-linking is an option to improve the stability of the PAA/PAH films, which our findings suggest is a necessary treatment if these specific materials are desired for use.

CONCLUSIONS

Our findings suggest that careful analysis of materials is required to reveal potential problems for in vivo biosensor coating applications; it is not sufficient to combine two multilayers with desirable properties and assume they will combine independently to provide the dual function. Along with the desired diffusion control, the susceptibility of underlying multilayers to environmental influence must be considered. In the case of our study on glucose diffusion, it was revealed that weak−weak PEMs should be not be used to control transport because of their irregular behavior under physiological conditions, even though they offer superior diffusion resistance. Application of a terminal layer of protein-resistant material does not substantially affect total film permeability—because of the much lower relative diffusivity, this characteristic is determined by the underlying films. Despite the lower permeability to glucose compared to strong−weak films, weak−weak films exhibited large variation in permeability after protein exposure, even when PEG surface coatings were applied. In contrast, strong−weak pairs were more robust and maintained stable diffusion control when exposed to proteins. Thus, multilayers of strong−weak pairs should be used to achieve and maintain the desired flux balance, which may require deposition of thicker layers to obtain lower permeability. It is also possible that more complex combinations of strong−weak with intervening weak−weak domains could be considered. This will be one aspect of our future work on these interesting and useful nanofilm systems.

Acknowledgment. This work is supported by National Science Foundation (BES-060037) and National Institutes of Health (R01 EB000739). Ellipsometry was performed at the TAMU Materials Characterization Facility. The FE-SEM imaging was completed at the TAMU Microscopy and Imaging Center (MIC); the assistance of Mr. Tom Stephens of MIC is gratefully acknowledged. The FE-SEM acquisition was supported in part by the National Science Foundation (DBI-0116835).

Supporting Information Available: QCM results of film deposition, SEM images of nanoilms before after serum exposure, ellipsometry for nanofilm thickness on porous alumina substrate, change in glucose diffusivity in nanofilms after FBS exposure for 24 h, and diffusion coefficient calculation (PDF). This material is available free of charge via the Internet at http://pubs.acs.org.

REFERENCES AND NOTES

(1) Gough, D. A.; Lucisano, J. Y.; Tse, P. H. S. *Anal. Chem.* **1985**, *57*, 2351–2357.
(2) Wilson, R.; Turner, A. P. F. *Biosens. Bioelectron.* **1992**, *7*, 165–185.
(3) Bremer, T. M.; Edelman, S. V.; Gough, D. A. *Diabetes Technol. Ther.* **2001**, *3*, 409–418.
(4) Stucker, M.; Struk, A.; Altmeyer, P.; Herde, M.; Baumgartl, H.; Lubbers, D. W. *J. Physiol.* **2002**, *538*, 985–994.
(5) Evans, N. T.; Naylor, P. F. *Respir. Physiol.* **1966**, *2*, 61–72.
(6) Wu, C.-C.; Yasukawa, T.; Shiku, H.; Matsue, T. *Sens. Actuators, B* **2005**, *110*, 342–349.
(7) Rego, R.; Caetano, N.; Vale, R.; Mendes, A. *J. Membr. Sci.* **2004**, *244*, 35–44.
(8) Rivera, H.; Cole, A.; Santiago-Aviles, J.; Smith, D. *Sensors* **1994**, *11*, 72–73.
(9) Salimi, A.; Roushani, M. *Electrochem. Commun.* **2005**, *7*, 879–887.
(10) Zhang, Y.; Hu, Y.; Wilson, G. S.; Moatti-Sirat, D.; Poitout, V.; Reach, G. *Anal. Chem.* **1994**, *66*, 1183–1188.
(11) Lu, J.; Do, I.; Drzal, L. T.; Worden, R. M.; Lee, I. *ACS Nano* **2008**, *2*, 1825–1832.
(12) Desai, T. A.; Hansford, D. J.; Leoni, L.; Essenpreis, M.; Ferrari, M. *Biosens. Bioelectron.* **2000**, *15*, 453–462.
(13) Uehara, H.; Kakiage, M.; Sekiya, M.; Sakuma, D.; Yamonobe, T.; Takano, N.; Barraud, A.; Meurville, E.; Ryser, P. *ACS Nano* **2009**, *3*, 924–932.
(14) Decher, G. *Science* **1997**, *277*, 1232–1237.
(15) *Multilayer Thin Films: Sequential Assembly of Nanocomposite Materials*, 1st ed.; Decher, G., Schlenoff, J. B., Eds.; Wiley-VCH: Weinheim, Germany, 2003; p 543.
(16) Liu, X.; Bruening, M. L. *Chem. Mater.* **2004**, *16*, 351–357.
(17) Miller, M. D.; Bruening, M. L. *Langmuir* **2004**, *20*, 11545–11551.
(18) Harris, J. J.; Stair, J. L.; Bruening, M. L. *Chem. Mater.* **2000**, *12*, 1941–1946.
(19) Stein, E. W.; Grant, P. S.; Zhu, H.; McShane, M. *J. Anal. Chem.* **2007**, *79*, 1339–1348.
(20) Stein, E. W.; Singh, S.; McShane, M. *J. Anal. Chem.* **2008**, *80*, 1408–1417.
(21) Jiang, C.; Wang, X.; Gunawidjaja, R.; Lin, Y.-H.; Gupta, M. K.; Kaplan, D. L.; Naik, R. R.; Tsukruk, V. V. *Adv. Funct. Mater.* **2007**, *17*, 2229–2237.
(22) Battle, A. R.; Valenzuela, S. M.; Mechler, A.; Nichols, R. J.; Praporski, S.; di Maio, I. L.; Islam, H.; Girard-Egrot, A. P.; Cornell, B. A.; Prashar, J.; Caruso, F.; Martin, L. L.; Martin, D. K. *Adv. Funct. Mater.* **2009**, *19*, 201–208.
(23) Zhang, X.; Sharma, K. K.; Boeglin, M.; Ogier, J.; Mainard, D.; Voegel, J.-C.; Mély, Y.; Benkirane-Jessel, N. *Nano Lett.* **2008**, *8*, 2432–2436.
(24) Volodkin, D.; Arntz, Y.; Schaaf, P.; Moehwald, H.; Voegel, J.-C.; Ball, V. *Soft Matter* **2008**, *4*, 122–130.
(25) Swiston, A. J.; Cheng, C.; Um, S. H.; Irvine, D. J.; Cohen, R. E.; Rubner, M. F. 2008, *8*, 4446−4453.
(26) Guillaume-Gentil, O.; Akiyama, Y.; Schuler, M.; Tang, C.; Textor, M.; Yamato, M.; Okano, T.; Vörös, J. *Adv. Mater.* **2008**, *20*, 560–565.
(27) Berthelemy, N.; Kerdjoudj, H.; Gaucher, C.; Schaaf, P.; Stoltz, J.-F.; Lacolley, P.; Voegel, J.-C.; Menu, P. *Adv. Mater.* **2008**, *20*, 2674–2678.

(28) Ladam, G.; Schaaf, P.; Decher, G.; Voegel, J.-C.; Cuisinier, F. J. G. *Biomol. Eng.* **2002**, *19*, 273–280.
(29) Anderson, J. M. In *Biomaterials Science*, 1st ed.; Ratner, B., Hoffman, A., Schoen, F., Lemons, J., Eds.; Academic Press: New York, 1996; Vol. 1, pp 165—173.
(30) Jeon, S. I.; Lee, J. H.; Andrade, J. D.; De Gennes, P. G. *J. Colloid Interface Sci.* **1991**, *142*, 149–158.
(31) Lutkenhaus, J. L.; Olivetti, E. A.; Verploegen, E. A.; Cord, B. M.; Sadoway, D. R.; Hammond, P. T. 2007, *23*, 8515—8521.
(32) Zahr, A. S.; Davis, C. A.; Pishko, M. V. 2006, *22*, 8178—8185.
(33) Heuberger, R.; Sukhorukov, G.; Vörös, J.; Textor, M.; Möhwald, H. *Adv. Funct. Mater.* **2005**, *15*, 357–366.
(34) Elbert, D. L.; Hubbell, J. A. *Chem. Biol.* **1998**, *5*, 177–183.
(35) Pasche, S.; DePaul, S. M.; Voros, J.; Spencer, N. D.; Textor, M. *Langmuir* **2003**, *19*, 9216–9225.
(36) Jeon, J.; Panchagnula, V.; Pan, J.; Dobrynin, A. V. *Langmuir* **2006**, *22*, 4629–4637.
(37) Kato, N.; Schuetz, P.; Fery, A.; Caruso, F. *Macromolecules* **2002**, *35*, 9780–9787.
(38) Balachandra, A. M.; Dai, J.; Bruening, M. L. *Macromolecules* **2002**, *35*, 3171–3178.
(39) Schuetz, P.; Caruso, F. *Adv. Funct. Mater.* **2003**, *13*, 929–937.
(40) Sauerbrey, G. *Z. Phys. A: Hadrons Nucl.* **1959**, *155*, 206–222.
(41) Raabo, E.; Terkildsen, T. C. *Scand. J. Clin. Lab. Invest.* **1960**, *12*, 402–407.
(42) Michel, R.; Pasche, S.; Textor, M.; Castner, D. G. *Langmuir* **2005**, *21*, 12327–12332.
(43) Huang, N.-P.; Michel, R.; Voros, J.; Textor, M.; Hofer, R.; Rossi, A.; Elbert, D. L.; Hubbell, J. A.; Spencer, N. D. *Langmuir* **2001**, *17*, 489–498.
(44) Chen, H.; Hu, X.; Zhang, Y.; Li, D.; Wu, Z.; Zhang, T. *Colloids Surf., B* **2008**, *61*, 237–243.
(45) Ladam, G.; Gergely, C.; Senger, B.; Decher, G.; Voegel, J.-C.; Schaaf, P.; Cuisinier, F. J. G. *Biomacromolecules* **2000**, *1*, 674–687.
(46) Salloum, D. S.; Schlenoff, J. B. *Biomacromolecules* **2004**, *5*, 1089–1096.
(47) Shiratori, S. S.; Rubner, M. F. *Macromolecules* **2000**, *33*, 4213–4219.
(48) Tanchak, O. M.; Barrett, C. J. *Chem. Mater.* **2004**, *16*, 2734–2739.
(49) Gergely, C.; Bahi, S.; Szalontai, B.; Flores, H.; Schaaf, P.; Voegel, J.-C.; Cuisinier, F. J. G. *Langmuir* **2004**, *20*, 5575–5582.
(50) Mendelsohn, J. D.; Barrett, C. J.; Chan, V. V.; Pal, A. J.; Mayes, A. M.; Rubner, M. F. *Langmuir* **2000**, *16*, 5017–5023.
(51) Fery, A.; Scholer, B.; Cassagneau, T.; Caruso, F. *Langmuir* **2001**, *17*, 3779–3783.
(52) Hiller, J. A.; Mendelsohn, J. D.; Rubner, M. F. *Nat. Mater.* **2002**, *1*, 59–63.
(53) Zhai, L.; Nolte, A. J.; Cohen, R. E.; Rubner, M. F. *Macromolecules* **2004**, *37*, 6113–6123.

AM900673R